Since January 2020 Elsevier has created a COVID-19 resource centre with free information in English and Mandarin on the novel coronavirus COVID-19. The COVID-19 resource centre is hosted on Elsevier Connect, the company's public news and information website.

Sustainable Cities and Society 73 (2021) 103102

Contents lists available at ScienceDirect

Sustainable Cities and Society

journal homepage: www.elsevier.com/locate/scs

Experimental study on the control effect of different ventilation systems on fine particles in a simulated hospital ward

Xiangfei Kong [a], Chenli Guo [a], Zhang Lin [b], Shasha Duan [a], Junjie He [a], Yue Ren [a], Jianlin Ren [a,*]

[a] School of Energy and Environmental Engineering, Hebei University of Technology, Tianjin, China
[b] City University of Hong Kong Shenzhen Research Institute, Shenzhen, China

ARTICLE INFO

Keywords:
Cross-infection
Side return air distribution
Ventilation performance
Particulate matter
Exposure control

ABSTRACT

In recent years, a large number of respiratory infectious diseases (especially COVID-19) have broken out worldwide. Respiratory infectious viruses may be released in the air, resulting in cross-infection between patients and medical workers. Indoor ventilation systems can be adjusted to affect fine particles containing viruses. This study was aimed at performing a series of experiments to evaluate the ventilation performance and assess the exposure of healthcare workers (HW) to virus-laden particles released by patients in a confined experimental chamber. In a typical ward setting, four categories (top supply and exhaust, side supply and exhaust) were evaluated, encompassing 16 different air distribution patterns. The maximum reduction in the cumulative exposure level for HW was 70.8% in ventilation strategy D (upper diffusers on the sidewall supply and lower diffusers on the same sidewall return). The minimum value of the cumulative exposure level for a patient close to the source of the contamination pertained to Strategy E (upper diffusers on the sidewall supply and lower diffusers on the opposite sidewall return). Lateral ventilation strategies can provide significant guidance for ward operation to minimizing the airborne virus contamination. This study can provide a reference for sustainable buildings to construct a healthy indoor environment.

1. Introduction

Since December 2019, the COVID-19 outbreak has occurred in many countries worldwide. The COVID-19 pandemic has considerably affected the sustainable development of cities and societies and raised concerns regarding the influence of regulated indoor environments on human health. Many infected patients have been hospitalized to seek medical care. Through testing, most of these patients were found to be carriers of the infectious virus through testing and were thus sent to the hospitals for quarantine treatment. However, certain infected patients who did not exhibit any notable symptoms likely engaged in social activities in public places. Therefore, ensuring social distancing in public places is particularly important to control the spread of the virus (Su et al., 2021; Sun, & Zhai, 2020). To alleviate the problem of insufficient hospital beds caused by an excessive number of patients being sent to hospitals for treatment, Wuhan, as one of the cities severely affected by the pandemic, established 16 square cabin hospitals for treating patients with mild symptoms (Fang et al., 2020; Wang et al., 2020; Zhang et al., 2020). Wuhan's temporary hospitals, which resemble a centralized clinic with diagnostic functions, can accommodate thousands of beds. However, in this scenario, those thousands of patients may be in the same room, viruses may be transmitted from patients to medical staff and among patients (Bukhari et al., 1993; Ge et al., 2020; Liu et al., 2020).

Larger droplets (> 5 μm) and smaller aerosols (≤ 5 μm) that contain viruses are released into the indoor air through patients' breathing, talking and coughing (Dhand & Li, 2020; Gralton, Tovey, McLaws & Rawlinson, 2011). If these particles are directly inhaled or fall on mucous membranes, droplet or aerosol infections may occur (Atkinson & Wein, 2008; Wong K. et al., 2010). It has been experimentally shown that the ventilation system impacts the air flow pattern in a room and thus influences the effective removal of water droplets and bacteria (Chen & Zhao, 2010; Guo et al., 2021; Wan & Chao H., 2007).

Many researchers have focused on the effective removal of fine particles from the air (Feng & Cao, 2019; Feng, Yang & Zhang, 2020), prediction of indoor pollutants and indoor intelligent ventilation systems (Ren & Cao, 2020; Ren & Cao, 2019). By combining the research mechanism of fine particulate matter removal with the mechanism of influence of ventilation systems on the indoor airflow, many experiments have been conducted to examine the control effect of airflow

* Corresponding author.
E-mail address: jlren@hebut.edu.cn (J. Ren).

https://doi.org/10.1016/j.scs.2021.103102
Received 21 April 2021; Received in revised form 12 June 2021; Accepted 14 June 2021
Available online 17 June 2021

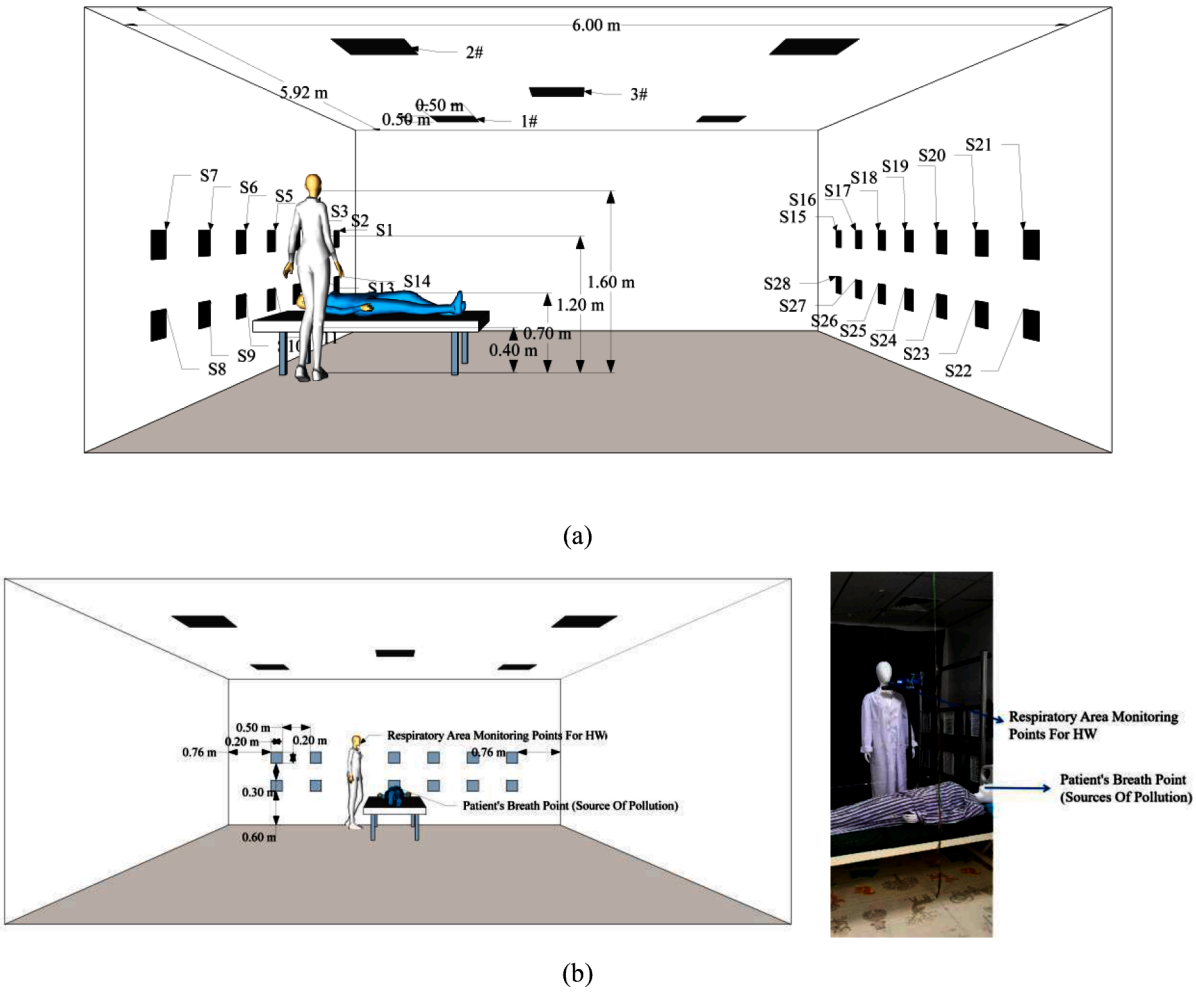

Fig. 1. (a) Front view of the chamber. The white and blue mannequin simulate a healthcare worker (HW) and patient (P) as the source of pollution, respectively. (b) Right side view of the chamber. The figures on the left and right represent a schematic and actual image, respectively.

patterns on fine particulate matter in isolation wards.

Many existing articles have highlighted different ventilation forms (Cao et al., 2014; Melikov, 2016; Yang et al., 2019), such as displacement ventilation (DV), mixed ventilation (MV), underfloor air distribution (UFAD), wall air ventilation (WAV), protective occupancy ventilation (POV), laminar air flow (LAF), and personalized ventilation (PV). The following ventilation systems have been recommended for hospital wards: DV, downward ventilation and MV (Qian, Li, Nielsen, & Hyldgaard, 2008; Yau, Chandrasegaran, & Badarudin, 2011). Qian and colleagues (Qian et al., 2006; Qian & Li, 2010) studied three different ventilation systems, including MV, downward ventilation and DV, to control the exhaled droplet nuclei of patients. The spatial distribution of the corresponding concentration was measured. The authors experimentally and computationally investigated the fate of breathing particles in a full-size, six-bed isolation chamber with vents at various locations. The results showed that the existing ventilation design of isolation chambers is not completely effective in removing fine and large breathing particles. Studies have suggested that increasing the ventilation rates to reduce the possibility of infection transmission may incur higher energy and financial costs. Therefore, this study suggests an intelligent and low-cost risk control strategy that combines infection prevention with energy conservation (Wang, Huang, Feng, Cao & Haghighat, 2021).

To examine the contamination level pertaining to different ventilation systems with exposure to the human body, significant research has been performed considering different distances and heights, humidity and breathing cases, to formulate an exposure index correlating the location and distance pertaining to the infected individuals; moreover, several studies have attempted to examine the effect of tracer gas concentration changes on the exposure risk. In these articles (Ai et al., 2019; Berlanga, Olmedo, et al., 2018; Berlanga, de Adana, et al., 2018; Cao et al., 2015; Liu, Li, Nielsen, Wei & Jensen, 2017; Manuel Villafruela, Castro, Francisco San Jose & Saint-Martin, 2013; Olmedo et al., 2012; Qian et al., 2006), the influence of different ventilation and filtration systems on the pollutant control was reported. The studies were primarily aimed at examining different air distribution patterns (DV, MV, and protected area ventilation), ventilation frequencies (ACH), and different relative positions between patients and infected persons that corresponded to a high risk of infection transmission. However, these studies did not examine the effects of exposure to infection when the return vent was near the source of the contamination. To the best of our knowledge, extremely few experimental studies have focused on the relative location of the return air outlet and the patient's respiratory area.

Under the stratified ventilation mode, the supply and return air inlets are located on the sidewalls of the room. Therefore, in this mode, the return air inlets are closer to the patients' respiratory area than in other ventilation modes. Fong et al. conducted experimental studies on the thermal sensation in MV, DV and stratified ventilation rooms. Compared with MV and DV, floor ventilation consumed less energy (Fong, Lin, Fong, Chow & Yao, 2011). Lin et al. studied the particle dispersion in classrooms under DV and stratified ventilation under three typical

Table 1
The supply and return air locations of the 16 ventilation systems considered in this study.

Strategy No.	Air supply	Air return
1-(A)		1#
2	3#	2#
3		1# and 2#
4-(B)		S8-S14
5	3#	S11
6		S1-S7
7		S4
8-(C)	S5-S10	
9	S1-S7	1# and 2#
10	S8-S14	
11-(D)	S1-S7	S8-S14
12-(E)	S1-S7	S22-S28
13-(F)	S15-S21	S8-S14
14-(G)	S8-S14	S15-S21
15	S1-S7	S15-S21
16	S8-S14	S22-S28

scenarios through a numerical simulation. The results of the study showed that the concentration of particulate matter in the respiratory zone was significantly lower than that in DV. These findings indicated that the risk of pathogenic bacteria inhalation in ground ventilation was lower than that in DV (Lin, Wang, Yao & Chow, 2012). Moreover, several studies (Cheng & Lin, 2015; Tian, Lin & Wang, 2010) were conducted on stratified ventilation, including the examination of the thermal comfort assessment, indoor stratified ventilation airflow characteristics, and transmission and infection performance in the classroom. The results showed that compared with MV and DV, stratified ventilation corresponded to a smaller blowing sensation, higher thermal comfort and more energy savings. Notable, the existing research on layered ventilation has mainly focused on the thermal comfort and energy consumption among other aspects, and extensive and targeted experimental research has not been conducted on its impact on the pollutant removal, especially in terms of the exposure of medical staff.

To obtain the appropriate ventilation strategy to reduce particulate matter exposure in hospital wards, we conducted experimental research, obtained a considerable amount of experimental data, and established a database. This paper experimentally compared the fine particle control effect of the following four categories of air distribution forms: (1) top air supply and top air exhaust adopted in general wards; (2) top air supply and side air return (close to the floor), while the wards adopt top air supply and side air exhaust (close to the patients' breathing area); (3) side return air and top exhaust air; and (4) side exhaust and side supply air. The experimental data can be used to assess the risk due to inhalation exposure of healthcare workers (HWs) and patients (Ps) to viral particles released by a P in the same ward. Moreover, the experimental results can provide a reference for the sustainable buildings in terms of establishing a healthy indoor environment.

2. Experimental Methods

2.1. Test chamber description

The experiment was conducted in a laboratory at Hebei University of Technology. The laboratory chamber was arranged in accordance with the requirements for intensive care units and infection units, specified in China's national standard (GB 50849-2014, GB 51039-2014). The laboratory chamber was 5.92 m long, 6.0 m wide and 2.8 m high. Five diffusers (#1-5, size: 0.5 × 0.5 m) were placed on the top ceiling of the chamber and 28 diffusers (#S1-S28; size: 0.2 × 0.2 m) were placed on the sidewall of the chamber. The locations of the diffusers are shown in Fig. 1.

According to the configuration of the experimental cabin, we studied four kinds of air supply and exhaust modes, namely, top air supply, top air supply side, side air supply, and side air supply side. The first type, that is, top supply air top exhaust air, can be subdivided into 3 types (Strategies 1, 2 and 3). The case with the exhaust at the top supply side can be subdivided into 4 types (Strategies 4, 5, 6 and 7). The case with the exhaust at the top of the side supply air can be subdivided into 3 types (Strategies 8, 9 and 10). The case with the side supply air side exhaust air can be subdivided into 6 cases (Strategies 11, 12, 13, 14, 15 and 16). Detailed schemes of the 16 different ventilation systems are presented shown in Table 1, and the corresponding system diagrams are shown in Fig. 2 and Table 1.

2.2. Experiment setup

The following experimental measurements were conducted in this study. First, we measured the indoor temperature and air velocity distributions under different ventilation modes. The blowing sense and ventilation performance of the Ps and the HWs were calculated and compared. Second, the exposure of the HWs to pollutants exhaled by Ps in a single room under different airflow patterns was analyzed. Effects of the P-exhaled contaminants on different exposures to infection among Ps in multiple wards were examined. Third, based on the results of the study, the optimal ventilation mode that could rapidly discharge pollutants from the P's breathing zone in the event of an infectious disease and to reduce the risk of cross-infection during the implementation of isolation in the space was determined. The experimental database including the temperature, air velocity and fine particle distribution under different ventilation systems provided in this study can be used to verify the numerical simulation results in further studies. To quantify the transport of particles generated by Ps, two experimental scenarios were considered. The first scenario was aimed at assessing the effect of particles generated by Ps on HWs. The second scenario was designed to study the transport of particles generated by a P to other Ps in the same hospital ward. In the two experimental scenarios, different numbers of dummy mannequins were used to simulate the human body. The dummies had the same size and shape and were not heated in these two experimental scenarios.

In the first scenario, the laboratory was simulated as a single-P infectious monitoring ward, to which a specific P was assigned; a certain HW was assigned to perform medical examinations and nursing activities for P. The locations of the HW and P are shown in Fig. 1. Two mannequins, with a height of 1.80 m and surface area of approximately 1.7 m2, were used. Since the height of the dummy experimental model was 1.8 m, the height of the respiratory area was approximately 1.6 m.

In the second scenario, three mannequins were placed in the experimental chamber to simulate a ward with three Ps. The distance between the beds satisfied the requirements for multibed wards in hospitals in China. The locations of the three mannequins in this experiment are shown in Fig. 3. In both scenarios, incense was set near the mouth of the Ps to represent the particle source. This research involved the following three steps. First, the temperature and wind velocity flow fields of the 16 different ventilation systems were measured and recorded. Second, the processes of pollutant removal and exposure to medical personnel were simulated in a single ward. Third, the exposure among the Ps was simulated in a three-person ward.

Temperatures at 11 heights were recorded at nine locations, as shown in Fig. 4. By controlling the temperature of the ventilation and air conditioning system in the experimental chamber, the indoor temperature was maintained at 24±1°C, and the average indoor temperature was approximately 24°C. The indoor wind speeds of the different ventilation systems were measured using a hot-wire anemometer, and the four height planes corresponded to 0.4 m, 0.7 m, 1.2 m, and 1.6 m. Each plane had 24 measurement points. The measurement points for the indoor air velocity are shown in Fig. 5. The specific coordinates of the measurement points are summarized in Tables S1 and S3.

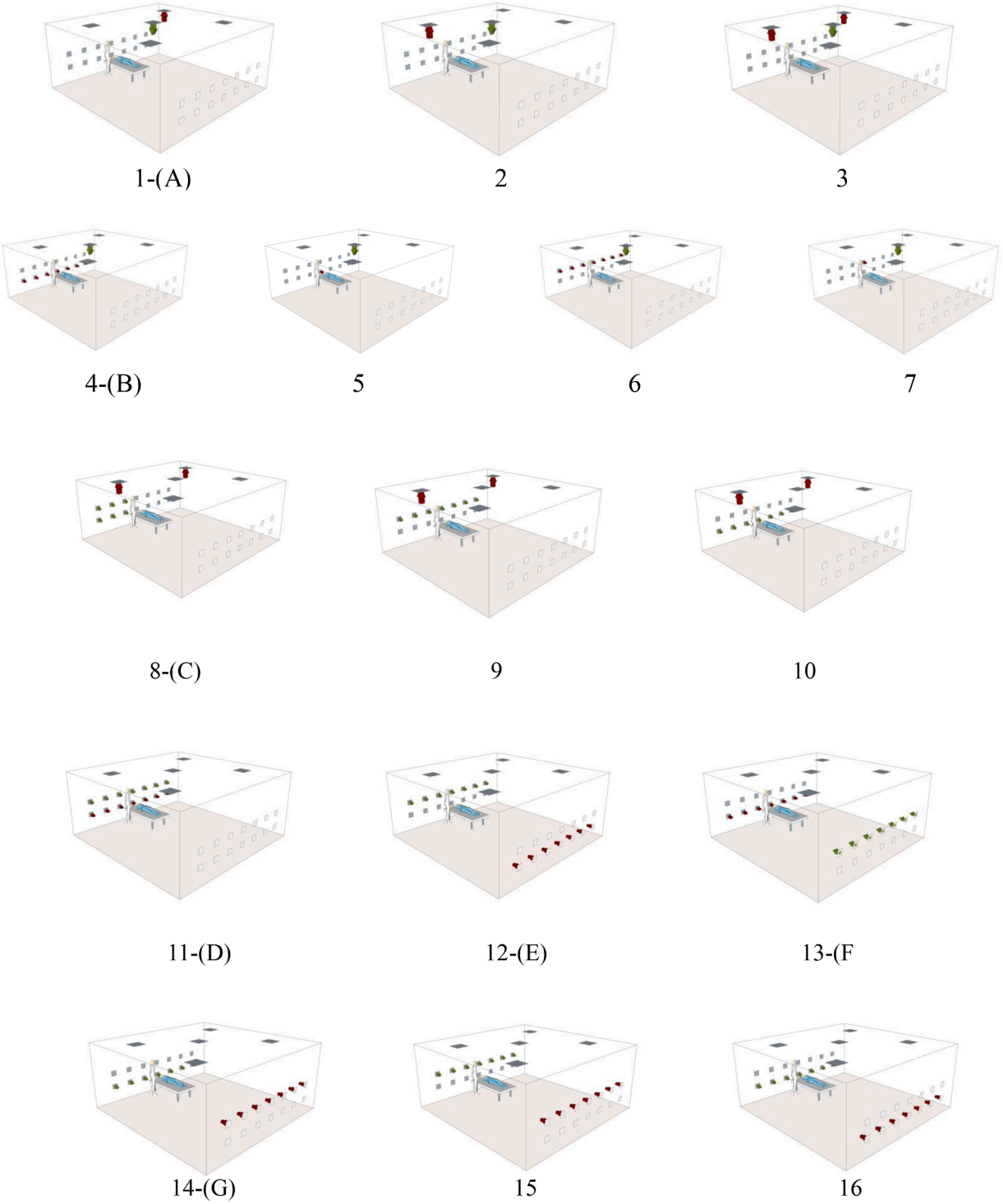

Fig. 2. Sixteen ventilation systems (White and blue dummies simulate HW and P as the source of the pollution, respectively.) (The green and red arrows indicate the air input and output, respectively.)

2.3. Ventilation system and configurations

Experiments were conducted for different ventilation configurations that provided clean air and exhaust through the celling or sidewall diffusers. A ventilation rate of 10 ACH was set in these strategies. The same air flow rate was maintained in all experiments to ensure repeatability of the trials and comparability of the environmental conditions with those in a real ward. For different tuyere shapes, different wind speed measurement methods were used. For rectangular and circular tuyeres, 16 and 5 points were selected to measure the wind speed, respectively. After the stable operation of the fan, measure multiple groups of data were measured, and the average value was considered.

2.4. Measurement instruments

The temperature, wind speed, and fine particulate concentration were recorded at different heights at three different measurement points. During the experiment, the temperature field and air flow field

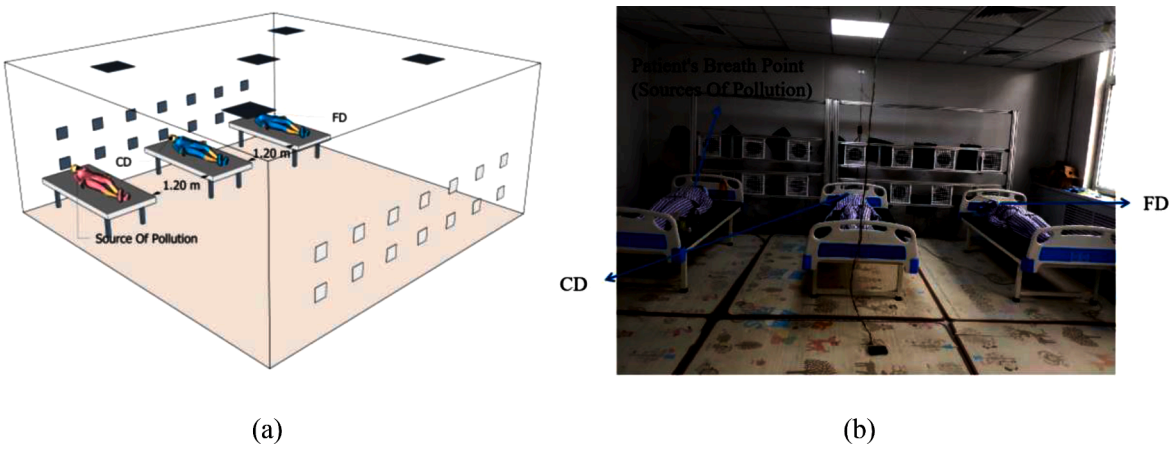

Fig. 3. Equidistant view of a simulated multi-P room in the test room, showing the distance between beds and the measurement points for P's respiratory area at a location close to (CD) and far from (FD) the source of the pollution. (a) Schematic (The pink and blue dummies mimic the P as the source of the pollution and an infected P.) (b) Real image.

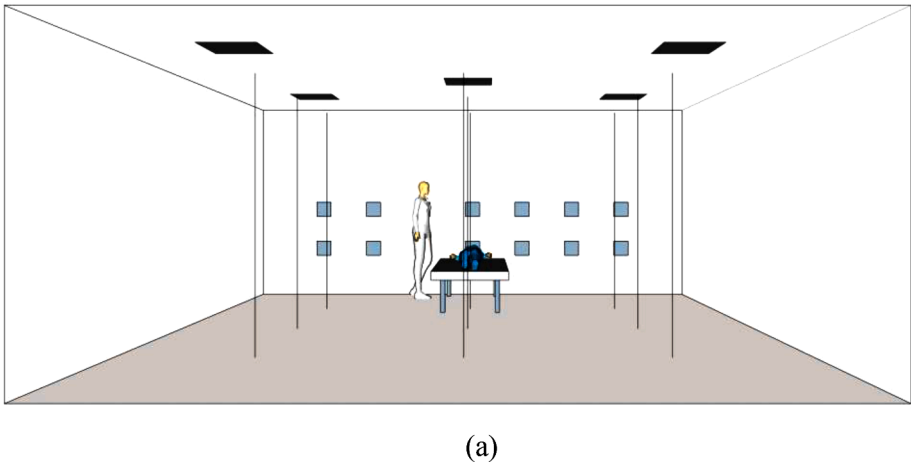

Fig. 4. The location of the temperature measurement points. (a) Schematic of the right side view; (b) Real image, showing only a few measurement points.

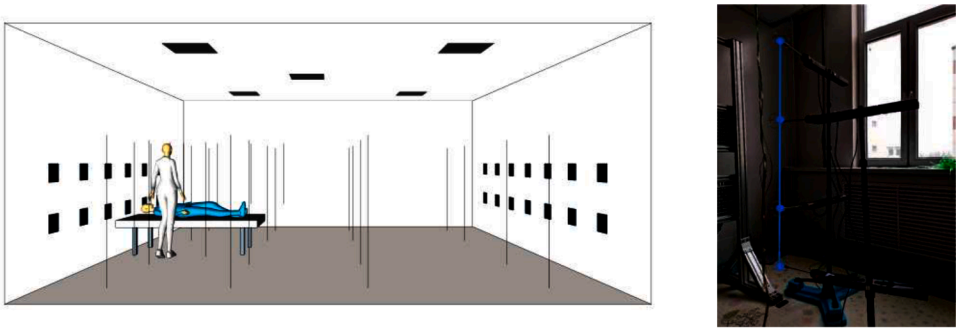

(a) (b)

Fig. 5. Location of the air velocity measurement point. (a) Schematic of the front view; (b) Real image, showing only a few measurement points.

were measured (as shown in Figs. 4 and 5). The heights of the particulate matter concentrations in the laboratory were 0.7 m and 1.6 m, respectively. The net height of the hospital bed was 0.53 m. In the actual use, a mattress and bed sheet with a height of approximately 0.1 m were expected to be added. Therefore, the height of the bed used by a P was 0.63 m, and the height of the breathing area when the P lay on the bed was approximately 0.7 m. The height of the sidewall tuyere in the laboratory was 0.7 m. In addition, according to previous articles, the height of the breathing area for a sitting human was approximately 1.2 m.

The ambient temperature probe included a T-type thermocouple with an accuracy of ±0.1°C in the range of -200°C to 260°C. Wind speed was measured using a hot wire anemometer measurement (TESTO440 MODE TYPE 06280152 SERIAL No. 61183753) with a range of 0.02 to 3.0 m/s and accuracy of ±0.07 m/s. The concentration of fine particulate matter was measured using a handheld airborne particle counter (TSI AEROTRAK MODEL 9306-V2) with a size range of 0.3 μm to 10.0 μm; the computation efficiency was 50% and 100% for 0.3 μm and > 0.45 μm, respectively. The particle counters used in this study could measure the number concentration of particles in the size ranges of 0.3-0.5 μm, 0.5-1.0 μm, 1.0-2.5 μm, 2.5-5.0 μm, 5.0-10.0 μm, and >10.0 μm. By comparing the $PM_{2.5}$ mass concentration value with the previously reported values, a more convincing conclusion could be obtained. The $PM_{2.5}$ mass concentration was be calculated using the following equation (Ren, Wade, CorsiL. & Novoselac, 2020):

$$M_{PM2.5} = \frac{1}{6}\pi\rho\left(d_1^3N_1 + d_2^3N_2 + d_3^3N_3\right) \times 10^{-6} \quad (1)$$

where $M_{PM2.5}$ is the $PM_{2.5}$ mass concentration (μg/m^3); ρ is the density of test dust used in this study, 1000 kg/m^3; N_1, N_2, and N_3 are the number concentrations of particles in the size ranges of 0.3-0.5 μm, 0.5-1.0 μm, and 1.0-2.5 μm, respectively (particles/m^3); and d_1, d_2, and d_3 are the median mass concentration sizes of the three size bins (μm).

2.5. Thermal comfort indices

The steps listed in ISO EN 7730-2005 were adopted to determine the thermal comfort index at different HW and P measurement points. The operating temperatures of the Ps and HWs were obtained to evaluate the thermal comfort. The values corresponded to HWs for the people standing and Ps for the people sitting after the steady-state conditions were achieved in the lab. Because the current standard does not provide a way to capture these indicators for a person lying down, the closest body position was selected. The HW was standing near the hospital bed in which P was lying. Due to the geometry of the bed, the flow pattern and thermal conditions at the P position could be different. However, the range of variations in the draft was required to not violate the wider thermal comfort range. Thus, the gust discomfort was assessed as the local gust discomfort.

In general, discomfort due to draught may be expressed as the percentage of people predicted to be affected by the draught. The draught rate (*DR*) was calculated using the following equation (model of draught):

$$DR = \left(34 - t_{a,l}\right)\left(\bar{v}_{a,l} - 0.05\right)^{0.62}\left(0.37\cdot\bar{v}_{a,l}\cdot T_u + 3.14\right) \quad (2)$$

For $\bar{v}_{a,l} < 0.05m/s$: use $\bar{v}_{a,l} = 0.05m/s$;

For $DR > 100\%$: use DR = 100% where $t_{a,l}$is the local air temperature in degrees Celsius; here, 20°C to 26°C. $\bar{v}_{a,l}$is the local mean air velocity in meters per second;here, <0.5 m/s; and $T_u$is the local turbulence intensity in percent points; here, 10% to 60% (if unknown, 40% may be used).

The model can be applied to people with low (mainly sedentary) activity levels, with the thermal sensation for the whole body being close to neutral, to predict the draught at the neck. At the level of the arms and feet, the model can overestimate the predicted DR. The value range of DR is based on the DR value specified in the *ISO 7730-2005* thermal environment classification. *ISO7730-2005* has different DR value ranges for different categories (A, B and C), among which the minimum DR range is <10.

2.6. Ventilation performance indices

Because the droplets produced by a patient's cough carry the virus and these droplets are of the order of nano- and micrometers, the droplets can be replaced by tiny particles. Under the given laboratory conditions, we conducted two kinds of experiments, namely, static and dynamic experiments. The static experiment was conducted to test the attenuation effect of different ventilation systems on the fine particulate matter with different particle sizes. In this experiment, the measurement points were arranged in the respiratory areas of the P and HW, the indoor central point (IC) and the location of the return air outlet, and the process monitoring and recording were conducted for these measurement points. The test steps were as follows: First, fine particulate matter was generated indoors. A certain amount of sandalwood dust was used to simulate the release of fine particulate matter indoors. In the static test, the particles were produced by the burning of sandalwood. The burning process was strictly timed to ensure that the same number of equisized particles were produced. The dominate aerodynamic diameter of the particles produced by sandalwood combustion was between 0.3 and 10.0 μm. In the static experiment, the particles were released through combustion at the center of the indoor ground. Second, four stirring fans were operated to ensure a uniform particle distribution. In different locations of the room, the number of particles was continuously monitored by operating the fans for different durations, and the distribution of the particles was confirmed to be uniform through analysis. Each process of the experiment was subjected to strict time control. Third, the fine particles in the room were allowed to decay naturally and under different ventilation conditions. In addition, the experiment was

Table 2
Experimental temperature under different ventilation conditions.

Strategy No.	1	2	3	4	5	6	7	8
Average Temperature (°C)	23.4	23.4	25.3	24.2	24.7	24.0	23.9	24.3
Strategy No.	9	10	11	12	13	14	15	16
Average Temperature (°C)	24.3	25.3	23.6	23.8	24.2	24.6	23.8	23.9

repeated multiple times. The complete process lasted at least two hours.

The following equation can be used to calculate the attenuation effect of the number of fine particles (Ren & Liu, 2019):

$$C = C_0 \times exp(-kt) \tag{3}$$

$$k = k_e - k_n \tag{4}$$

where C is the real-time number of fine particles, #/m3; C_0 is the initial number of fine particles, #/m3; t is the decay time, h; k is the particle number decay rate constant, h−1; k_e and k_n represent the total and natural decay rate constants of the number of particles, h−1, respectively.

The dynamic experiment was divided into a single-P ward and multi-P ward simulation experiments. In the dynamic test, the particles were produced by sandalwood combustion. Each combustion process was time-controlled to ensure that the same size and number of equalized particles were produced. The sandalwood material adopted in the dynamic experiment was the same as that used in the static experiment; however, the shape, height and burn time of the sandalwood were different due to the consideration of the distance between the P's respiratory area and its surrounding location. The particles were burned and released at the position of P's mouth. The pollution source (P's mouth) released pollutants (fine particles) into the room. In the single-room simulation experiment, a P (blue dummy) and an HW (white dummy) were considered, as shown in Fig. 4. The relative positions of and distance between the entities as well as other information are also shown in Fig. 4. During the experiment, the concentration of fine particles at the inhalation point (nose) of the HW was monitored and recorded. The multi-P bed simulation experiment, as shown in Fig. 5, involved three Ps, one of whom was a pollutant source (pink dummy), and the other two were pollutant receivers (blue dummies). During the experiment, the concentration of fine particles at the inspiratory point (nose) of the infected Ps was monitored and recorded.

The average concentration in the inhaled airway of the HW indicated the average human expiratory concentration of source P and was defined as the inhalation fraction (*IF*) index, which could be calculated as follows:

$$IF = \frac{\int Q_{b,inh} c_{inh} dt}{\int Q_{b,exh} c_{exh} dt} \tag{5}$$

where $Q_{b,inh}$ and $Q_{b,exh}$ (l/min) are the breathing rates of the HW (target) and P (source) mannequins, respectively, similar to the considerations in this study, $C_{inh}$is the average contaminant concentration inside the inhalation airway of the HW mannequin, and C_{exh} is the average contaminant concentration emitted through P exhalation.

The exposure rate (*ER*) was determined by the *IF* and could be calculated as follows:

$$ER = (1 - IF) \times 100\% \tag{6}$$

Based on the background experiment, the particle count changes in the background and nonbackground experiments were integrated over a certain period, and the reduced exposure rate (RER) was obtained by comparing the reductions in the nonbackground and background experiments.

The cumulative exposure level (*CEL*) was determined by N_t and could be calculated as follows:

$$CEL = \int_{t_0}^{t} N_t dt \tag{7}$$

where N_t(#/s) is the number of particle concentrations measured over time at a measurement point. The CEL was obtained by integrating the exposure time of the particle. The obtained experimental data (data of particle changes with time) were plotted and integrated, corresponding to the integration of the particle concentration changes over time.

3. Results

3.1. Air temperature distribution under different ventilation systems

During the experiment, the indoor temperature was monitored and recorded, and the average value of the experimental results was considered to calculate the DR. As 1 and 2 in Table 2 were tested on the same day, the temperature was the same. The temperature pertaining to various working conditions in the Table 2 was considered to calculate DR. The temperature data in the table were averaged. The temperature differences between the experimental groups could be attributed to the differences in the outdoor temperature, even though the unit was set to be at the same temperature to minimize the deviation. The detailed temperature data are provided in Table S4.

3.2. Air flow field under different ventilation system conditions

During the experiment, we conducted a continuous measurement for 5 min after the operation of the unit (wind speed of tuyere) was stabilized, with a set of data obtained per second, leading to 300 sets of data. A total of 24 corresponding measurement points were considered, which were located in 4 height planes. Next, the average value and variance of the data were calculated. Finally, Origin 2018 softwere was used to plot the measured data to obtain the speed cloud map. Fig. 6 shows seven (Strategies A-G) velocity clouds at a height of 0.7 m and a set of superimposed clouds (H) at heights of 0.4 m, 0.7 m, 1.2 m, and 1.6 m. Strategy 1(A) was selected, and the wind speed results for the four considered heights are shown in Fig. 6.

3.3. DR

The experimental data obtained by measuring the temperature field and flow field of the air speed were processed and analyzed. A height of 0.7 m represented the height of the P lying on the hospital bed, and the DR at this height could fully explain the P's DR. The results show that the DR at the positions of 0.7 m and 1.6 m are different under different working conditions.

As shown in Fig. 7, most of the DR values are no more than 10, indicating that the occupants (HW and P) have a slight feeling of blowing air under the 16 ventilation systems. In the case of the side return air system (Strategy 4-7,11-16), although DR is slightly higher in certain cases, the blowing sensation is relatively weak. The experimental conditions can thus satisfy the requirements of the human body for thermal sensation.

The comparison between Fig. 7(a) and (b) shows that the air blowing sensation, which is considered to be significant at a height of 0.7 m, is slightly larger than that at a height of 1.6 m, mainly because when the

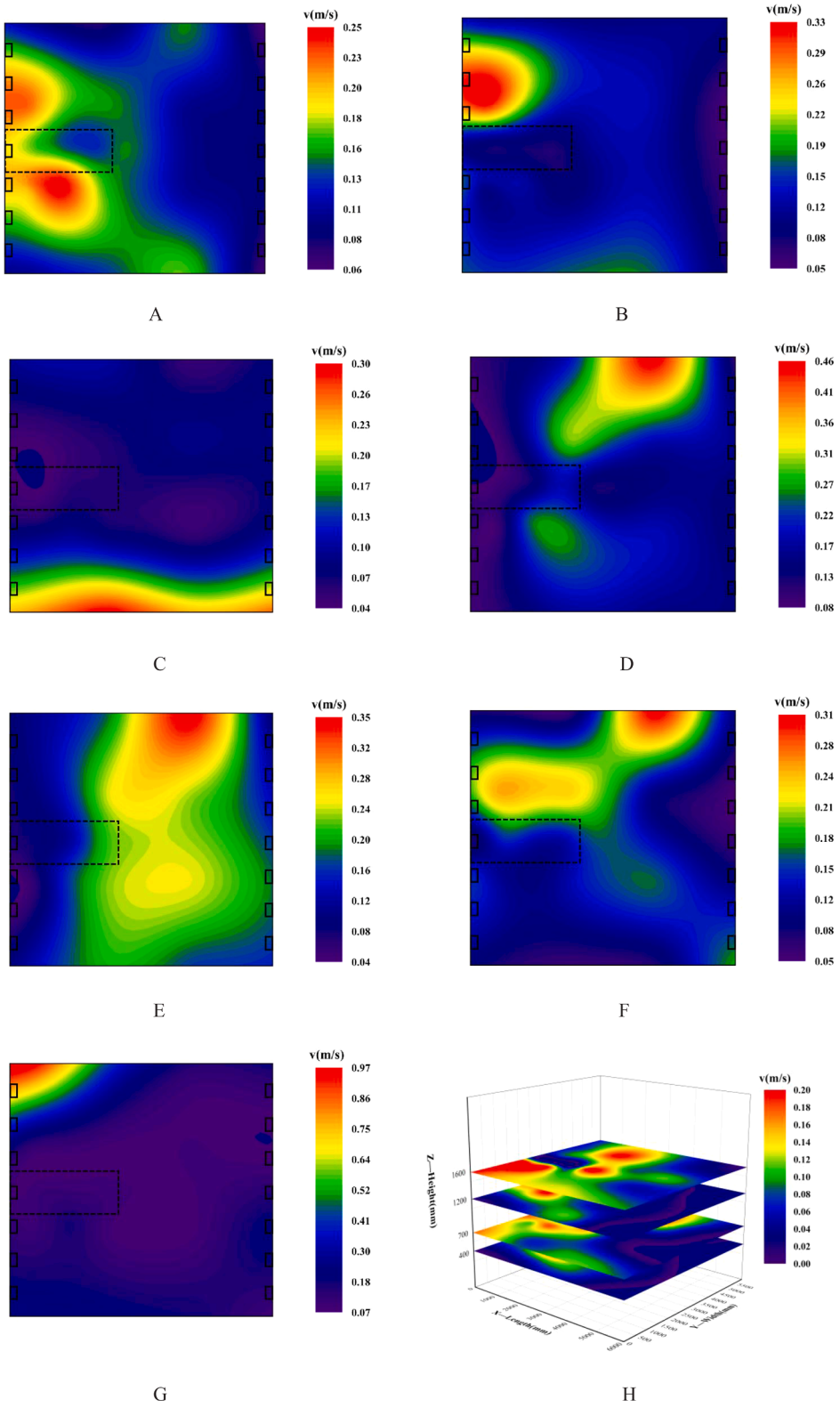

Fig. 6. A-G and H velocity clouds. In A-G, the black dotted line frame represents the hospital bed, indicating the location of the hospital bed; the black solid line frame represents the sidewall air outlet, indicating the location of the air outlet. H is a two-dimensional figure, which shows the length, width and height of H after simplifying the experimental chamber.

side air supply is at the sidewall, the exhaust outlet under the sidewall is at a height of 0.7 m, and the air supply distance is relatively small. The height of 1.6 m represents the height of the respiratory area of an HW standing beside P's bed. The DR value can represent the sense of hair blowing on the head and neck of the HW. Basically, the DR value is less than 10, indicating that the HW has only a slight sense of hair blowing. After comparison, seven experimental schemes (Strategies A-G) with notable effects and extreme representation were selected.

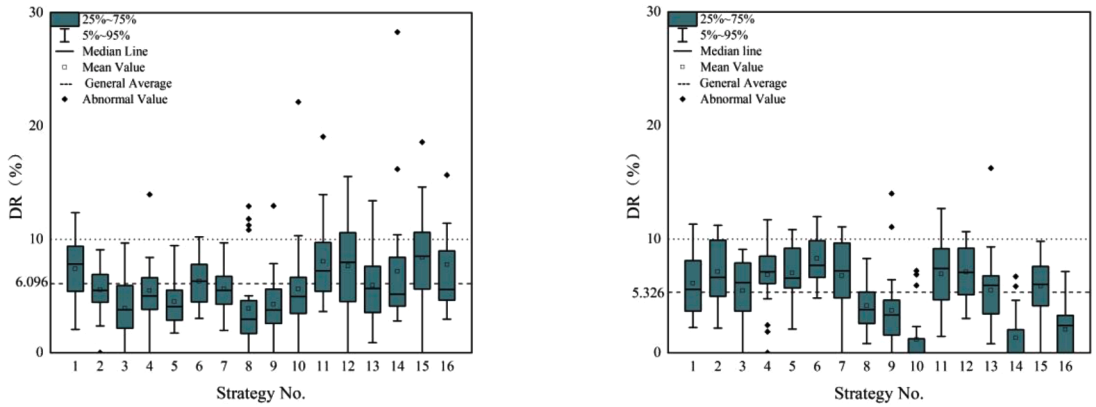

Fig. 7. (a) The draught rate (DR) under the operation of 16 ventilation systems in a plane with a height of 0.7 m; (b) DR under operating conditions of 16 ventilation systems in a plane with a height of 1.6 m. The figure shows the median line, mean value, general average of all the data at this height, and outliers.

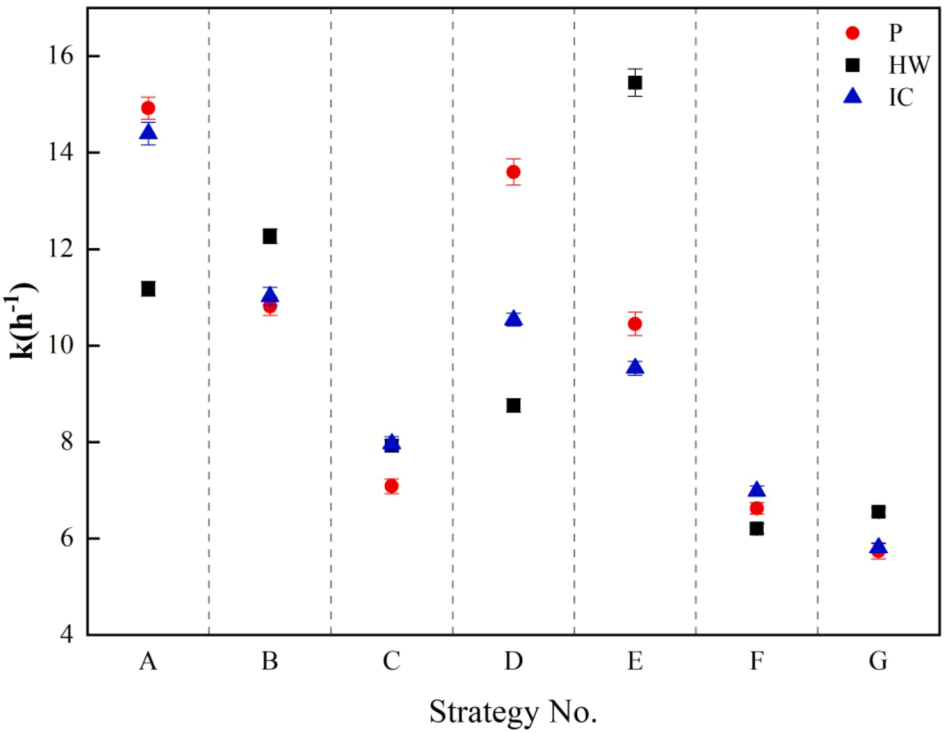

Fig. 8. The k values under seven ventilation system conditions (Strategies A-G). Measurement points: respiratory areas of P and HW and the indoor center point (IC).

Since this paper tested only the air blowing sensation without the experimental measurement of the predicted mean vote (PMV) and predicted percentage dissatisfied (PPD), we obtained the corresponding results by comparison with the data reported in other papers. According to the existing articles (Khodakarami & Nasrollahi, 2012; Verheyen, Theys, Allonsius & Descamps, 2011) and *ASHRAE* on the thermal comfort of the ward, the PPD% value was 8.8, and PMV value was 0.4±0.2. A study (Tian, Lin, Liu & Wang, 2008) on the ventilation room thermal comfort found that the subjects exhibited PPD% values of 50 and a PMV value of approximately 0. According to these results, the value range of category B (DR<20) corresponds to *ISO 7730-2005*. Moreover, in this study, the DR value during the whole experimental process was no more than 20, except for certain outliers. Therefore, this experimental condition could satisfy the required thermal sensation.

3.4. Ventilation rate

Using the measured data and according to Eq. (4) presented in Section 2.6, the k value was obtained. The calculation results are shown in Fig. 8. Fig. 8 shows the calculation results of particles with aerodynamic diameters greater than 0.3 μm (sum of particle counts for all channels of the instrument).

Fig. 8 shows the ventilation effect of the ventilation systems. Strategies A, B, D, and E exhibit a high ventilation performance, while Strategies C, F, and G exhibit a low ventilation performance. As far as P is concerned, Strategy A corresponds the highest ventilation efficiency, followed by Strategy D. The result for Strategy A may be attributed to the rapid air exchange rate in P's respiratory area when the air returns at the top of the top supply air, and thus, the ventilation effect in the respiratory area is high. The result of Strategy D can be attributed to the side supply air and side return air. The duration of such airflows is small,

Table 3
Comparison of different aerodynamic diameters (μm) in different ventilation systems.

(a) HW and IC

	>0.3	0.3-0.5	0.5-1.0	1.0-3.0	3.0-5.0	5.0-10.0	>10.0
A	△						
B	△△	△△		△			
C							
D	√√	√√	√√ △△	√√ △△	√√ △△	√√ △△	√√ △△
E				√			
F			△				
G							

(b) CD, FD and S

	>0.3	0.3-0.5	0.5-1.0	1.0-3.0	3.0-5.0	5.0-10.0	>10.0
A							
B	○○	○○	○○ ☆	○○ ☆☆	○○	○○	○○
C				□			
D					□□ ○ ☆☆	○ ☆☆	
E	□□ ☆☆	□□ ☆☆	□□ ☆☆	□□			
F						□□	□□ ☆☆
G							

and the airflow distance is small. In terms of the location of the HW, Strategy E exhibits the highest ventilation efficiency, followed by Strategy B, likely because the distance between the return air outlet and HW is small and the airflow distance is small. The reason for the higher k value in Strategies D and E may be thatin these strategies, clean air is sent to the room through upper diffusers on the sidewall (diffusers close to the breathing area), owing to which the air near the breathing area is promptly refreshed.

The clean air delivery rate (CADR) has been examined in many papers, and different values of CADR have been reported. In COVID-19-related studies (Christopherson, Yao, Lu, Vijayakumar & Sedaghat, 2020; Zhao, Liu & Chen, 2020), the values of CADR (m^3/h) were 300 and 361. In another study, the test result of CADR (m^3/h) was approximately 300-700. In this study, (Ren & Liu, 2019), CADR of the same significance could be obtained by using the k value. Since the volume of the experimental chamber was 5.92 m × 6.0 m × 2.8 m=99.5 m^3, the value of CADR could be calculated to be 500-1600 m^3/h. After comparison, the overall k value in this study was noted to be larger, which corresponds to a higher air purification effect.

3.5. Exposure to contaminants

The dynamic experiment simulated private rooms and multiple wards. The following table compares the exposure of the respiratory zones of HW, IC, and 2 Ps (CD and FD) with different aerodynamic diameters under 7 ventilation system conditions (Strategies A-G).

In Table 3, the presence of two symbols (e.g., $\sqrt{\sqrt{}}$) indicates the minimum value of the total particle count for the cumulative settlement that occurred after the fan and particle release of the air conditioner stabilized. The presence of a single symbol (e.g., $\sqrt{}$) indicates the value within 5% of the minimum value. The symbol ($\sqrt{}$) represents the cumulative count of the particles near the respiratory area of the HW. Similarly, the symbol (△) corresponds to the IC, the symbols (□) and (○) correspond to the respiratory area for CD and FD, respectively; and the symbol (☆) represents the sum (S) of the values of the respiratory areas for CD and FD.

Through the comparison of the different particle sizes under the same strategy, it was noted that the cumulative counts of particles in different particle sizes are different. In general, the channel value (aerodynamic particle size >0.3 μm) has a clear representation, and thus, certain graphs are plotted and presented with the channel value data (aerodynamic particle size >0.3 μm). The table indicates that in terms of the cumulative count of particles near the HW respiratory zone, the minimum value corresponds to Strategy D, followed by Strategy E; For the cumulative count of particles near the IC, the minimum value corresponds Strategies D and B In terms of the cumulative count of particles near the respiratory zone of CD, the minimum value appeared in Strategy B, followed by Strategy D For the cumulative count of particles near the FD respiratory zone, the minimum value appeared in Strategy E. The comparison of different ventilation systems, indicated that Strategies B, D, and E correspond to a low exposure risk.

The data were monitored and recorded throughout the experiment. We chose several sets of data to be presented. Fig. 9 shows the variation of the pollutant particle number concentration in the HW respiratory zone and CD and FD respiratory zones in the single ward in the simulated dynamic experiment. The particle count in the figure was the total value of the instrument channel (>0.3 μm). BE denotes the background experiment; Strategies A-D represent the different ventilation systems listed in Table 1.

The particle counts data in Fig. 9 changed all the times, and several outliers were present in the data owing to uncertain and uncontrollable factors during the experiment. Nevertheless, the overall trend of the data is clear: pollutants are released from the source location (P's breathing area; after a certain duration, the ventilation system is operated under different conditions to remove the indoor pollutants. Over time, pollutants in the HW respiratory zone increase in BE but decrease in Strategies A-D, and the rate of decrease is different.

Using Eqs. (6) and (7) presented in Section 2.6, the experimental data were calculated and processed to obtain the corresponding results, which plotted as graphs of the RER and CEL.

In Fig. 10, HW represents the respiratory area of HW, CD represents the respiratory area of patients close to the pollution source, FD represents the respiratory area of patients far from the pollution source, and AT represents the average values of HW, CD, and FD. In Fig. 11, BE represents the background experiment, and HW, CD and FD have the same meanings as those in Fig. 10.

As shown in Fig. 10, for the HW, Strategy D has the largest value of 70.8%, followed by Strategy E with a value of 69.4%, and the three worst groups are Strategies A, B, and G. For CD, Strategy E has the highest value, followed by Strategy C, and Strategies A, F and G are the three worst groups. For FD, Strategy B has the largest value, followed by Strategy C, and the three worst groups are Strategies A, F, and G. Overall, the value of RER are larger for Strategies D and E, intermediate for Strategies B and C, and small for Strategies A, F and G. A smaller RER corresponds to a smaller exposure reduction rate.

The possible reasons for the phenomenon observes in Fig. 10 are as follows. First, due to the different relative positions and heights of HW, CD and FD in the experimental chamber, the experimental results are slightly different. Second, the side air return method leads to a rapid reduction in the pollutant levels in the area near the return air outlet, thereby increasing the relative exposure reduction in the area.

As shown in Fig. 11, for the HW, Strategies D and E have small values, while Strategies A, C and G have large values. For CD, Strategies C, D, and E have small values, while Strategies A and F have large values. For FD, Strategies B, D, and E have small values, while Strategies F and G have large values. The minimum value of CEL (1. E +06#/m^3), and the removal efficiency for HW is 31.7 and 70.9% in Strategy D, respectively; for CD, the corresponding values were 16.0 and 83.5% in Strategy E; and for FD, the corresponding values were 11.0 and 89.2% in Strategy B. A larger CEL corresponds to a greater the cumulative exposure and the greater the risk of exposure.

The reasons for this phenomenon may be as follows: First, the positions and heights of the HW, CD and FD are different from those of the tuyere, leading to different results in the experiment. Second, in Strategies A-G, with 7 different ventilation systems, the air velocity of the

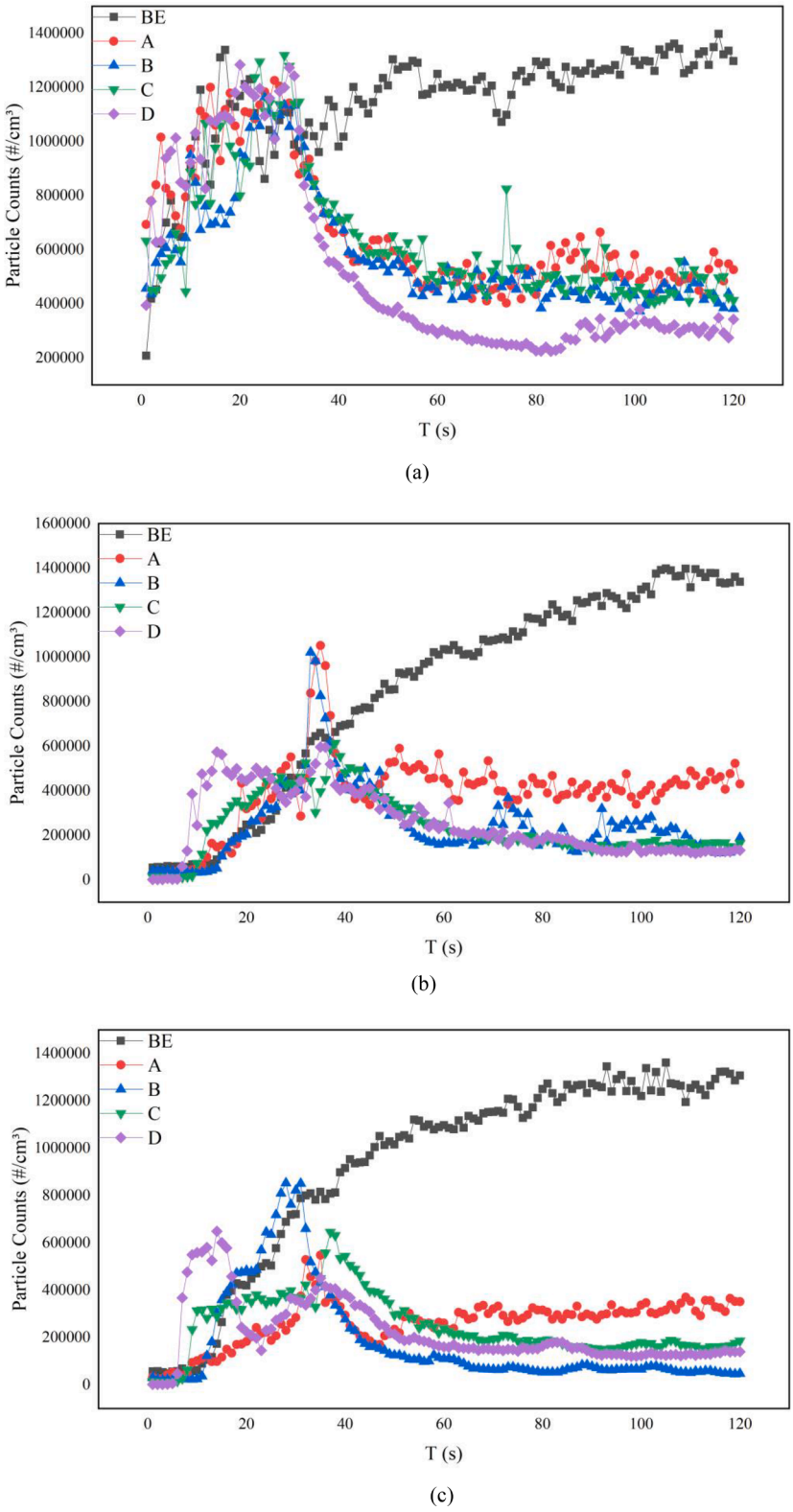

Fig. 9. Variation in the particle concentration in the (a) HW respiratory zone; (b) CD respiratory zone; (c) FD respiratory zone.

tuyere is different because the ventilation times are the same, but the area of the tuyere is not the same. Finally, different ventilation systems have different airflow paths.

3.6. Contaminant distribution

Eq. (2) in Section 2.4 was used to calculate and process the obtained data. As shown in Fig. 12 (a), Strategies D and E exhibit a higher removal effect of $PM_{2.5}$. In Fig. 12 (b), Strategies B and E exhibit superior effects. A greater value of $PM_{2.5}$ mass concentration in Fig. 12 corresponds to a

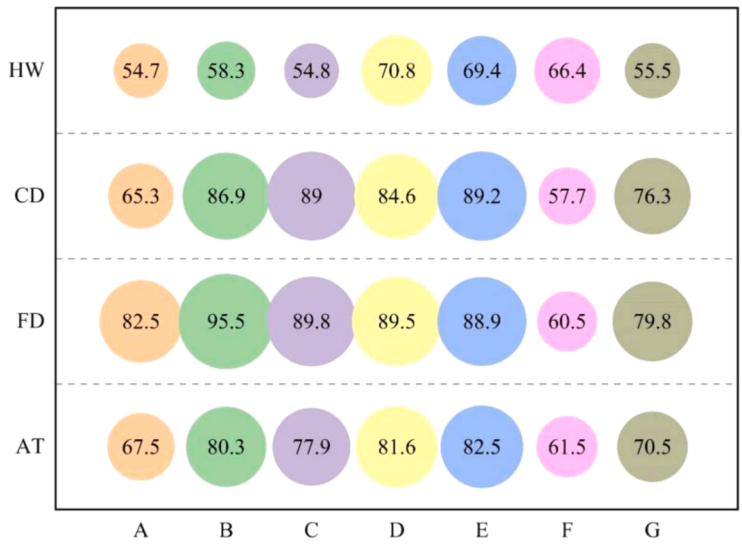

Fig. 10. The reduced exposure rate (%) under different ventilation modes.

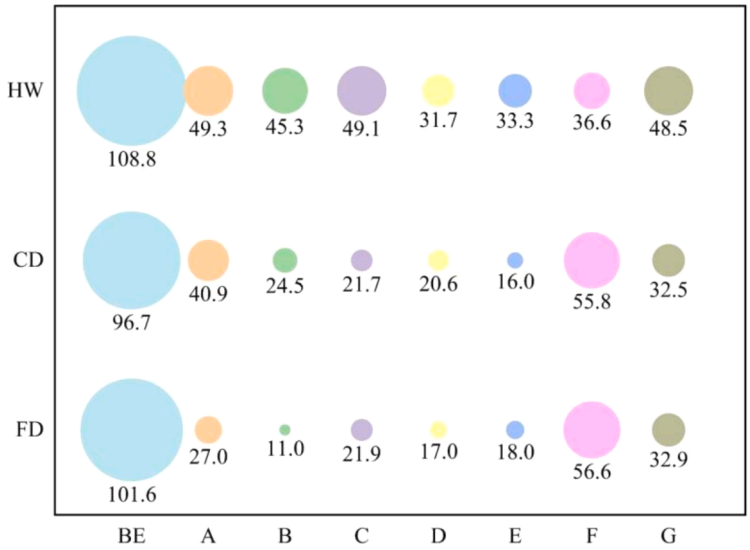

Fig. 11. The cumulative exposure level of the number of particles measured (1.0 E+06 #/m^3).

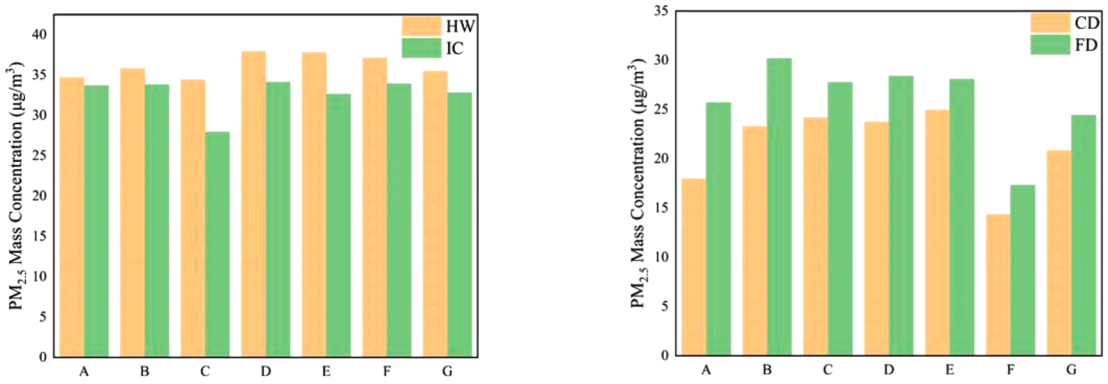

Fig. 12. (a) The $PM_{2.5}$ mass concentrations (μg/m^3) of HW and IC (the interior center point); (b) $PM_{2.5}$ mass concentration (μg/m^3) of CD and FD.

higher $PM_{2.5}$ removal effect in the environment. The main reason for this phenomenon may be that different ventilation systems have different airflow paths, and pollution sources have different relative positions with respect to the air supply outlet and the air return outlet. In particular, for the side air return of Strategies B and D, the airflow path in this form is considerably reduced.

4. Discussion

The removal effect of particulate matter in wards was experimentally studied (Chao, Wan & To, 2008). In this paper, after revising the adopted mode, the predicted deposition rate of 1.5 μm droplets was reduced by 25%. Due to the advantage of gravity deposition, more than 95% of the ≥87.5 μm exhaled droplets were removed by deposition. The experimental results indicated that different ventilation systems have different effects on particulate emissions. When we processed the data, we used the average value of the experimental data, which may have underestimated the exposure.

The innovations of this study are as follows: a variety of air distribution forms and different forms of wards were compared; moreover, the temperature field, velocity field, and concentration field under different air distributions were accurately measured, and a large number of databases were established, which could be used for CFD verification of future studies focused on wards. The shortcomings of this study are as follows: the experiments were not repeated, and the measurement of the air flow field was conducted only a single ward; future studies can be aimed at examining the traversal through multiple wards. In addition, the mannequin was not heated in this study. The thermal plume generated by the mannequin is expected to affect the transport and removal of particles under different ventilation systems.

5. Conclusion

In a typical air configuration case study involving top and side supply and return air systems, experimental tests were conducted to determine the thermal comfort, ventilation performance, and pollutant exposure. According to the results of the experiments and comparison among the results, the following conclusions could be derived.

Most of the DR values are no more than 10, indicating that the occupants (HW and P) have a slight feeling of blowing air under the 16 ventilation systems. In the side return air system (Strategies 4-7,11-16), although the value of DR is slightly higher in certain case, the blowing sensation is relatively small. The experimental conditions can meet the requirements of the human body for thermal sensation.

The results of the cumulative exposure to local pollutants show that the adopted ventilation strategies adopted are effective. The maximum value of RER (%) for HW was 70.8 in Strategy D. The minimum CEL ($1.0E+06\ \#/m^3$) value for HW was 31.7 in Strategy D, and the removal efficiency was 70.9%.

Considering these results, it is considered that the side return air is a feasible ventilation strategy to replace top return air. In this strategy, indoor occupants can experience a high comfort and ventilation performance. Moreover, this strategy can effectively reduce the exposure of pollutants and enhance the filtration efficiency. However, according to the results, the air distribution in the room must be focused on.

Declaration of Competing Interest

The authors declare that they have no known competing financial interests or personal relationships that could have appeared to influence the work reported in this paper.

Acknowledgments

This study was supported by the Natural Science Foundation of Hebei Province, China (Grant No. E2020202147), Hebei Province Funding Project for Returned Scholars, China (Project No. C20190507), Fundamental Research Funds of Hebei University of Technology (Project No. JBKYTD2003) and Shenzhen Science and Technology Innovation Commission, China (Project No. JCYJ20170818095706389).

Supplementary materials

Supplementary material associated with this article can be found, in the online version, at doi:10.1016/j.scs.2021.103102.

References

Ai, Z. T., Huang, T., & Melikov, A. K. (2019). Airborne transmission of exhaled droplet nuclei between occupants in a room with horizontal air distribution. *Building and Environment, 163*, Article 106328.

Atkinson, M. P., & Wein, L. M. (2008). Quantifying the routes of transmission for pandemic influenza. *Bulletin of Mathematical Biology, 70*(3), 820–867.

Berlanga, F. A., de Adana, M. R., Olmedo, I., Villafruela, J. M., San Jose, J. F., & Castro, F. (2018). Experimental evaluation of thermal comfort, ventilation performance indices and exposure to airborne contaminant in an airborne infection isolation room equipped with a displacement air distribution system. *Energy and Buildings, 158*, 209–221.

Berlanga, F. A., Olmedo, I., de Adana, M. R., Villafruela, J. M., San Jose, J. F., & Castro, F. (2018). Experimental assessment of different mixing air ventilation systems on ventilation performance and exposure to exhaled contaminants in hospital rooms. *Energy and Buildings, 177*, 207–219.

Bukhari, S. S., Sanderson, P. J., Richardson, D. M., Kaufman, M. E., Aucken, H. M., & Cookson, B. D. (1993). Endemic cross-infection in an acute medical ward. *The Journal of hospital infection, 24*(4), 261–271.

Cao, G., Nielsen, P. V., Jensen, R. L., Heiselberg, P., Liu, L., & Heikkinen, J. (2015). Protected zone ventilation and reduced personal exposure to airborne cross-infection. *Indoor Air, 25*(3), 307–319.

Cao, G. Y., Awbi, H., Yao, R. M., Fan, Y. Q., Siren, K., Kosonen, R., & Zhang, J. S. (2014). A review of the performance of different ventilation and airflow distribution systems in buildings. *Building and Environment, 73*, 171–186.

Chao, C. Y. H., Wan, M. P., & To, G. N. Sze (2008). Transport and removal of expiratory droplets in hospital ward environment. *Aerosol Science and Technology, 42*(5), 377–394.

Chen, C., & Zhao, B. (2010). Some questions on dispersion of human exhaled droplets in ventilation room: answers from numerical investigation. *Indoor Air, 20*(2), 95–111.

Cheng, Y., & Lin, Z. (2015). Experimental study of airflow characteristics of stratum ventilation in a multi-occupant room with comparison to mixing ventilation and displacement ventilation. *Indoor Air, 25*(6), 662–671.

Christopherson, D. A., Yao, W. C., Lu, M., Vijayakumar, R., & Sedaghat, A. R. (2020). High-Efficiency Particulate Air Filters in the Era of COVID-19: Function and Efficacy. *Otolaryngology-Head and Neck Surgery, 163*(6), 1153–1155.

Dhand, R., & Li, J. (2020). Coughs and Sneezes: Their Role in Transmission of Respiratory Viral Infections, Including SARS-CoV-2. *American Journal of Respiratory and Critical Care Medicine, 202*(5), 651–659.

Fang, D. P., Pan, S. J., Li, Z. S., Yuan, T., Jiang, B. R., Gan, D., & Liu, Z. M. (2020). Large-scale public venues as medical emergency sites in disasters: lessons from COVID-19 and the use of Fangcang shelter hospitals in Wuhan, China. *BMJ Global Health, 5*(6), Article e002815.

Feng, Z., & Cao, S.-J. (2019). A newly developed electrostatic enhanced pleated air filters towards the improvement of energy and filtration efficiency. *Sustainable Cities and Society, 49*, Article 101569.

Feng, Z., Yang, J., & Zhang, J. (2020). Numerical optimization on newly developed electrostatic enhanced pleated air filters for efficient removal of airborne ultra -fine particles: Towards sustainable urban and built environment. *Sustainable Cities and Society, 54*, Article 102001.

Fong, M. L., Lin, Z., Fong, K. F., Chow, T. T., & Yao, T. (2011). Evaluation of thermal comfort conditions in a classroom with three ventilation methods. *Indoor Air, 21*(3), 231–239.

Ge, X. Y., Pu, Y., Liao, C. H., Huang, W. F., Zeng, Q., Zhou, H., Yi, B., Wang, A. M., Dou, Q. Y., Zhou, P. C., Chen, H. L., Liu, H. X., Xu, D. M., Chen, X., & Huang, X. (2020). Evaluation of the exposure risk of SARS-CoV-2 in different hospital environment. *Sustainable Cities and Society, 61*, Article 102413.

Guo, Y., Qian, H., Sun, Z., Cao, J., Liu, F., Luo, X., Ling, R., Weschler, L. B., Mo, J., & Zhang, Y. (2021). Assessing and controlling infection risk with Wells-Riley model and spatial flow impact factor (SFIF). *Sustainable Cities and Society, 67*, Article 102719.

Gralton, J., Tovey, E., McLaws, M.-L., & Rawlinson, W. D. (2011). The role of particle size in aerosolised pathogen transmission: A review. *Journal of Infection, 62*(1), 1–13.

Khodakarami, J., & Nasrollahi, N. (2012). Thermal comfort in hospitals - A literature review. *Renewable & Sustainable Energy Reviews, 16*(6), 4071–4077.

Lin, Z., Wang, J., Yao, T., & Chow, T. T. (2012). Investigation into anti-airborne infection performance of stratum ventilation. *Building and Environment, 54*, 29–38.

Liu, L., Li, Y., Nielsen, P. V., Wei, J., & Jensen, R. L. (2017). Short-range airborne transmission of expiratory droplets between two people. *Indoor Air, 27*(2), 452–462.

Liu, Z., Wang, L., Rong, R., Fu, S., Cao, G., & Hao, C. (2020). Full-scale experimental and numerical study of bioaerosol characteristics against cross-infection in a two-bed hospital ward. *Building and Environment, 186*, Article 107373.

Manuel Villafruela, J., Castro, F., Francisco San Jose, J., & Saint-Martin, J (2013). Comparison of air change efficiency, contaminant removal effectiveness and infection risk as IAQ indices in isolation rooms. *Energy and Buildings, 57*, 210–219.
Melikov, A. K. (2016). Advanced air distribution: improving health and comfort while reducing energy use. *Indoor Air, 26*(1), 112–124.
Olmedo, I., Nielsen, P. V., de Adana, M. R., Jensen, R. L., & Grzelecki, P. (2012). Distribution of exhaled contaminants and personal exposure in a room using three different air distribution strategies. *Indoor Air, 22*(1), 64–76.
Qian, H., & Li, Y. (2010). Removal of exhaled particles by ventilation and deposition in a multibed airborne infection isolation room. *Indoor Air, 20*(4), 284–297.
Qian, H., Li, Y., Nielsen, P. V., & Hyldgaard, C. E. (2008). Dispersion of exhalation pollutants in a two-bed hospital ward with a downward ventilation system. *Building and Environment, 43*(3), 344–354.
Qian, H., Li, Y., Nielsen, P. V., Hyldgaard, C. E., Wong, T. W., & Chwang, A. T. Y (2006). Dispersion of exhaled droplet nuclei in a two-bed hospital ward with three different ventilation systems. *Indoor Air, 16*(2), 111–128.
Ren, C., & Cao, S.-J. (2020). Implementation and visualization of artificial intelligent ventilation control system using fast prediction models and limited monitoring data. *Sustainable Cities and Society, 52*, Article 101860.
Ren, C., & Cao, S.-J. (2019). Incorporating online monitoring data into fast prediction models towards the development of artificial intelligent ventilation systems. *Sustainable Cities and Society, 47*, Article 101498.
Ren, J., & Liu, J. (2019). Fine particulate matter control performance of a new kind of suspended fan filter unit for use in office buildings. *Building and Environment, 149*, 468–476.
Ren, J., Wade, M., Corsi, R. L., & Novoselac, A. (2020). Particulate matter in mechanically ventilated high school classrooms. *Building and Environment, 184*, Article 106986.
Su, J., He, X., Qing, L., Niu, T., Cheng, Y., & Peng, Y. (2021). A novel social distancing analysis in urban public space: A new online spatio-temporal trajectory approach. *Sustainable Cities and Society, 68*, Article 102765.
Sun, C., & Zhai, Z. (2020). The efficacy of social distance and ventilation effectiveness in preventing COVID-19 transmission. *Sustainable Cities and Society, 62*, Article 102390.
Tian, L., Lin, Z., Liu, J., & Wang, Q. (2008). Numerical study of Indoor Air Quality and thermal comfort under stratum ventilation. *Progress in Computational Fluid Dynamics, 8*(7-8), 541–548.
Tian, L., Lin, Z., & Wang, Q. (2010). Comparison of gaseous contaminant diffusion under stratum ventilation and under displacement ventilation. *Building and Environment, 45*(9), 2035–2046.
Verheyen, J., Theys, N., Allonsius, L., & Descamps, F. (2011). Thermal comfort of patients: Objective and subjective measurements in patient rooms of a Belgian healthcare facility. *Building and Environment, 46*(5), 1195–1204.
Wan, M. P., & Chao, C. Y. H (2007). Transport characteristics of expiratory droplets and droplet nuclei in indoor environments with different ventilation airflow patterns. *Journal of Biomechanical Engineering-Transactions of the Asme, 129*(3), 341–353.
Wang, J., Huang, J., Feng, Z., Cao, S. J., & Haghighat, F. (2021). Occupant-density-detection based energy efficient ventilation system: Prevention of infection transmission. *Energy and Buildings, 240*, Article 110883.
Wang, K. W., Gao, J., Song, X. X., Huang, J., Wang, H., Wu, X. L., ... Cheng, Y. (2020). Fangcang shelter hospitals are a One Health approach for responding to the COVID-19 outbreak in Wuhan, China. *One Health*, 10, 100167.
Wong, B. C. K., Lee, N., Li, Y., Chan, P. K. S., Qiu, H., Luo, Z., & Yu, I. T. S. (2010). Possible Role of Aerosol Transmission in a Hospital Outbreak of Influenza. *Clinical Infectious Diseases, 51*(10), 1176–1183.
Yang, B., Melikov, A. K., Kabanshi, A., Zhang, C., Bauman, F. S., Cao, G., & Lin, Z. (2019). A review of advanced air distribution methods - theory, practice, limitations and solutions. *Energy and Buildings, 202*, Article 109359.
Yau, Y. H., Chandrasegaran, D., & Badarudin, A. (2011). The ventilation of multiple-bed hospital wards in the tropics: A review. *Building and Environment, 46*(5), 1125–1132.
Zhang, J. S., Wang, M. L., Zhao, M. M., Guo, S. S., Xu, Y., Ye, J., & Wan, J. (2020). The clinical characteristics and prognosis factors of mild-Moderate patients With COVID-19 in a mobile cabin hospital: A retrospective, single-center study. *Frontiers in Public Health, 8*, 264.
Zhao, B., Liu, Y., & Chen, C. (2020). Air purifiers: A supplementary measure to remove airborne SARS-CoV-2. *Building and Environment, 177*, Article 106918.